

# Experimental Activities in China

(June 2008)

YU Hongwei

*China Nuclear Data Center, China Institute of Atomic Energy*

The facilities were used for the nuclear data measurements and studies including the China's first experimental heavy water reactor, the HI-13 tandem accelerator, 600kV-Cockcroft-Walton accelerator and 5SDH-2 tandem accelerator located at CIAE and 4.5-MV Van de Graaff accelerator at Peking University and 300kV -Cockcroft-Walton accelerator at Lanzhou University. The China experimental fast reactor and China advanced research reactor, which are under construction at CIAE, will be used for nuclear data related research.

The following nuclear data measurement laboratories are included in china Nuclear Data Network: China Institute of Atomic Energy(CIAE), Peking University, Sichuan University, Lanzhou University and etc. The summarized activities are covered during recent years.

## 1. China Institute of Atomic Energy

### • GTAF(Gamma Total Absorption Facility) detector in CIAE

Since the requirement of the  $(n,\gamma)$  cross-section data is increasing strongly in ADS project, Nuclear Waste Transmutation and Nuclear Astrophysics, we have set up a new measurement method which get the  $(n,\gamma)$  cross-section by detecting the prompt gammas from the capture of neutrons.

The gamma total absorption facility was chosen as our main detector. The detector consists of 42 BaF<sub>2</sub> crystals of 15 cm length. Covering the full solid angle without any gaps requires two different crystal shapes, which can be seen in the fig.1. The shapes of the crystals are optimized in a way that they all cover the same solid angle, although they have different shapes. The volumes described above can be arranged to form a closed sphere with an inner radius of 10 cm and an outer radius of 25 cm.

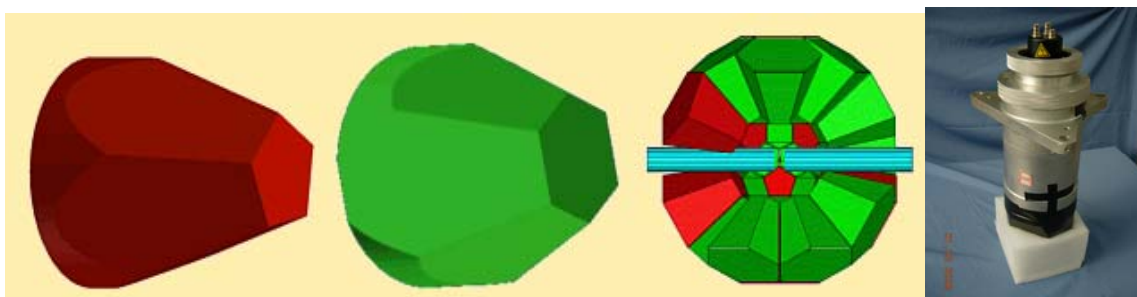


Figure 1 the different crystal shapes and the all crystals together (left)and the single detector module(right)



Fig.2: GTAF in CIAE

The external support is made by the stainless steel, the honey comb and support for crystals which are made by the Al. The construction of this system was finished last year at CIAE.

- **The experiment method study of decay data and measurement.**

The method study of decay data measurement has been performed with the examples of some shorter half-life nuclides at CIAE. Some primary results have been obtained and analyzed with the Table of Isotopes Eighth Edition for testing and checking the experimental method.

The half-life  $^{132}\text{I}$  was determined using a HPGE detector by place-replace method, calibrating efficiency was avoided by counting alternately at different places. In order to simplify the treatment of data, the real time of every counting interval was set the same. Two ways, iteration and teanslation, were adopted to deal with data. The obtained half-life value of  $^{132}\text{I}$  was  $(2.283 \pm 0.002)\text{h}$  which has been checked and provcn to be credible.

**Table Comparison of half-life value of  $^{132}\text{I}$**

Year	Author(s)	$t_{1/2}$ (h)
1954	Emery and Veall [1]	$2.259 \pm 0.008$
1955	Wahl [2]	$2.30 \pm 0.05$
1958	Keene and Mackenzie [3]	$2.292 \pm 0.007$
1965	Andersson and Rudstam [4]	$2.34 \pm 0.02$
1966	Marais and Haasbroek [5]	$2.2846 \pm 0.0004$
	This work	$2.283 \pm 0.002$

- **Measurement and evaluation the relative emission probabilities for high energy calibration of Ge detectors**

$^{56}\text{Co}$  and  $^{66}\text{Ga}$  with  $\gamma$ -ray energies covering the range of 0.84~3.55 and 0.68~4.81MeV respectively are important radionuclides for Ge detector calibration. Their evaluated and recommended relative  $\gamma$ -ray emission probabilities were done based on the main measurements of D.C.Camp et al. and M.E.Phelps et al. before 2000. The values reported by D.C.Camp, however, were systematically lower in high energies range (by as much as 30% for the 4806 keV  $\gamma$ -ray of  $^{66}\text{Ga}$ ) because the conclusion has been reached that above 2500 keV Ge detector efficiency curves do not decrease linearly with energy on a log-log scale since 1975. These measurements based on the assumption of almost linear extrapolation on a log-log plot of the efficiency curve between 2500 and 5000 keV were not corrected due to no high precise measurements. The experimental data measured after 2000 and recent evaluations of C.M.Baglin et al. and E.Browne et al. were analyzed and compared with our present measured and evaluated values for  $^{56}\text{Co}$  and  $^{66}\text{Ga}$

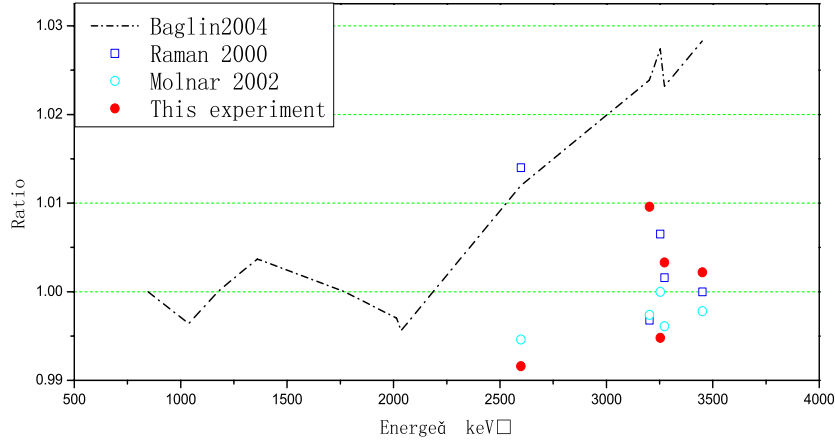


Fig.2 Comparison of present evaluation to Baglin's evaluation and modified measurements for  $^{56}\text{Co}$

The full efficiency curve used in the present measurement can be determined by the experiment and the Monte-Carlo calculation. Below 2.75MeV the efficiency curve was based upon the experimental data. Between 2.75 and 6.13MeV the efficiency curve was obtained from the Monte-Carlo calculation which has been validated by the experimental data at low energy region and agreed perfectly with the efficiency at 6.13MeV that was determined by the  $^{19}\text{F}(p, \alpha\gamma)^{16}\text{O}$  reaction.

By using the efficiency curve measured above, the new relative intensities were determined for the emitted  $\gamma$ -rays of  $^{56}\text{Co}$  and  $^{66}\text{Ga}$ . The final results are presented in Fig. 3 and Table 2 respectively. It's noted that our measurements are about 2% lower than other new measurements in high energy range.

**Table 2 Comparison of recent measured and evaluated relative  $\gamma$ -ray emission probabilities for  $^{66}\text{Ga}$**

$E_\gamma$ (keV)	Measurements				Evaluations		modified values			
	Molnar <sup>[10]</sup> (Budapest)	Raman <sup>[10]</sup>	Baglin <sup>[10]</sup> (Berkeley)	Present	Browne	Present	Molnar	Raman	Baglin	Present evaluation
833.6	15.92(6)	16.02(24)	15.94(14)	15.85(17)	15.94	15.92(5)				
1039.4	100.0(3)	100.0(16)	100.0(9)	100.0(5)	100.0	100.0				
1333.2	3.171(13)	3.17(5)	3.20(3)	3.15(2)	3.16	3.17(1)				
1918.8	5.360(23)	5.33(8)	5.44(6)	5.36(4)	5.38	5.37(2)				
2189.9	14.39(6)	14.54(21)	14.50(13)	14.12(12)	14.32	14.37(5)				
2422.9	5.072(24)	5.12(8)	5.15(6)	5.17(4)	5.08	5.10(2)				
2752.3	61.34(26)	61.2(8)	61.5(6)	60.80(40)	61.35	61.22(20)*	60.60(48)	60.84(91)	60.6(9)	60.71(6) <sup>b</sup>
3229.2	4.087(22)	4.06(8)	4.07(4)	4.00(6)	4.08	4.08(2) *	3.989(49)	4.01(9)	3.96(7)	3.99(1) <sup>b</sup>
3381.4	3.950(23)	3.96(8)	3.99(4)	3.83(4)	3.94	3.94(2) *	3.847(52)	3.91(9)	3.87(7)	3.86(2) <sup>b</sup>
4086.5	3.455(20)	3.38(8)	3.42(4)	3.36(5)	3.43	3.44(2) *	3.406(34)	3.35(9)	3.37(5)	3.37(1) <sup>b</sup>
4806.6	5.04(3)	4.93(11)	5.00(7)	4.99(8)	5.03	5.02(3) *	5.06(4)	4.94(11)	4.95(7)	4.99(3) <sup>b</sup>

### • Measurements of Neutron Emission Spectra of $n+^7\text{Be}$ and $n+^6,7\text{Li}$

The neutron emission double-differential cross sections(DDXs) of  $^9\text{Be}$  and  $^{6,7}\text{Li}$  were measured at incident neutron energies of 8.17 and 10.27 MeV on HI-13 Tandem Accelerator in CIAE. At 10.27 MeV, the influence of breakup source neutrons from  $\text{D}(d, np)$  reactions was eliminated by using the combination of abnormal and normal fast neutron TOF spectrometers. The measured TOF spectra were analyzed by detailed Monte-Carlo simulation and the DDXs were determined by comparing the measured TOF spectra

to simulated ones. The cross sections were normalized to n-p(normal geometry measurement) or n-C(abnormal geometry measurement) scattering measurement.

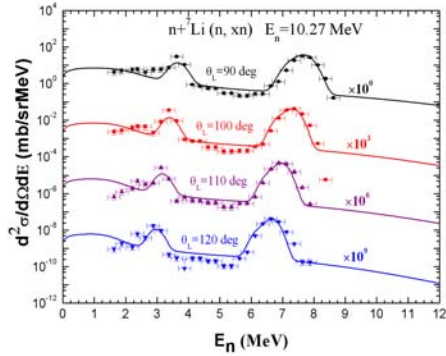


Fig.3 Measured DDXs result of  ${}^7\text{Li}$  at 10.27 MeV

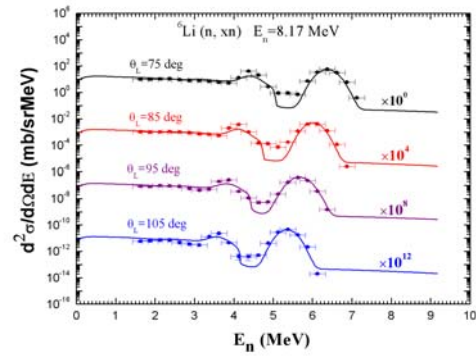


Fig.4 Measured DDXs for  ${}^6\text{Li}$  at 8.17 MeV

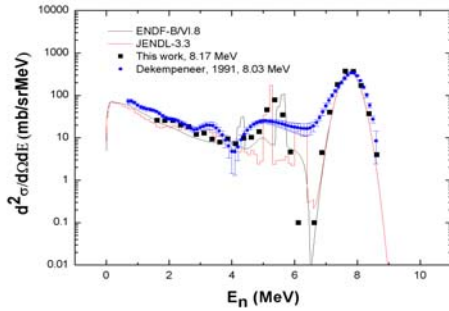


Fig. 5 DDXs result of  ${}^9\text{Be}$  at 40 degree for 8.17 MeV

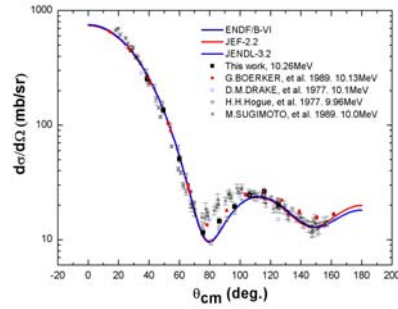


Fig. 6 Elastic scattering cross sections for  ${}^9\text{Be}$  at 10.27 MeV

### • Study of collision between ions and atoms.

The experiment was performed with the HI-13 tandem accelerator at the China Institute of Atomic Energy (CIAE). We tried to get the relations of scattering cross section energy, scattering cross section elements, inner shell ionization cross section energy, X-ray shift energy, and two-electron one-photon transition in inner shell etc. We measured C, Cu, F, O + Au, Cu, Cd, Fe, Mo, Nb, Ni, Ta.

## 2. Peking University

### • Differential and Angle-Integrated Cross Section Measurement for the ${}^{64}\text{Zn}(n,\alpha){}^{61}\text{Ni}$ Reaction

Differential and angle-integrated cross sections of the  ${}^{64}\text{Zn}(n,\alpha){}^{61}\text{Ni}$  reaction were measured at neutron energy 2.54, 4.00, 5.03, 5.5 MeV and 5.95 MeV by using a gridded ionization chamber. The experiment was performed at the 4.5 MV Van de Graaff accelerator of the Institute of Heavy Ion Physics, Peking University. Monoenergetic neutrons of 2.54 MeV were produced through the  $\text{T}(p, n){}^3\text{He}$  reaction with a solid Ti-T target, and those of 4.00 and 5.50 MeV were produced through the  $\text{D}(d, n){}^3\text{He}$  reaction with a deuterium gas target. Absolute neutron flux was determined by the  ${}^{238}\text{U}(n, f)$  reaction and a calibrated  $\text{BF}_3$  long counter. Present results are compared with existing data.

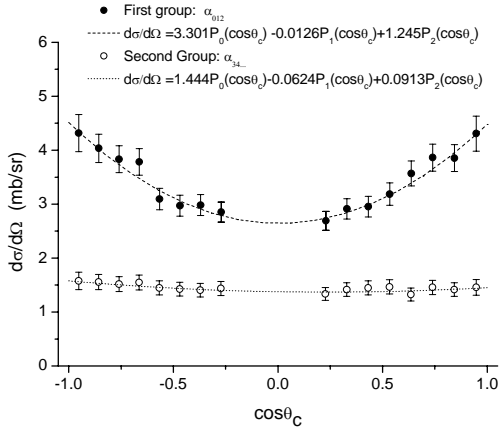


Fig. 7 The differential cross sections of  $^{64}\text{Zn}(n,\alpha)^{61}\text{Ni}$  reaction in the c.m. system at  $E_n=4.00$  MeV

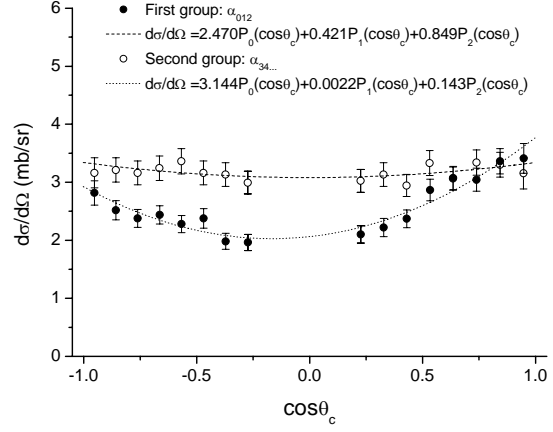


Fig. 8 The differential cross sections of  $^{64}\text{Zn}(n,\alpha)^{61}\text{Ni}$  reaction in the c.m. system at  $E_n = 5.50$  MeV

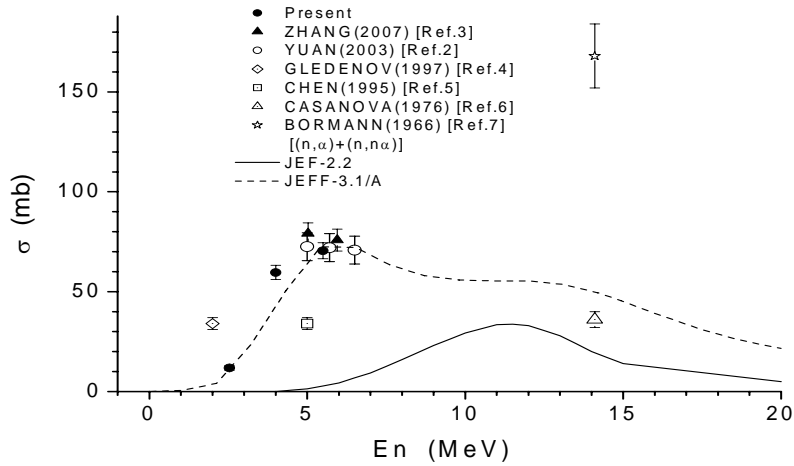


Fig. 9 Present cross sections of the  $^{64}\text{Zn}(n,\alpha)^{61}\text{Ni}$  reaction compared with existing data.

### • Measurement of cross sections for the $^{147}\text{Sm}(n,\alpha)^{144}\text{Nd}$ reaction

Cross sections of the  $^{147}\text{Sm}(n,\alpha)^{144}\text{Nd}$  reaction were measured at  $E_n = 5.0$  and  $6.0$  MeV. A twin gridded ionization chamber was used as charged particle detector and two large area  $^{147}\text{Sm}_2\text{O}_3$  samples back to back were employed. Experiments were performed at the 4.5 MV Van de Graaff accelerator of Peking University. Neutrons were produced through the  $\text{D}(d,n)^3\text{He}$  reaction with a deuterium gas target. Absolute neutron flux was determined by a small  $^{238}\text{U}$  fission chamber.

### • Measurement of neutron capture cross sections for $^{141}\text{Pr}$

Cross sections of  $^{141}\text{Pr}(n,\gamma)^{142}\text{Pr}$  reaction are measured at neutron energies of 0.54, 1.09 and 1.59 MeV using the activation method. The activities of the products are counted with a high resolution HPGe detector g-ray spectrometer. The neutron fluence is determined by  $^{197}\text{Au}(n,\gamma)^{198}\text{Au}$  reaction cross sections. The errors of the measured results are  $\pm 6-7\%$ .

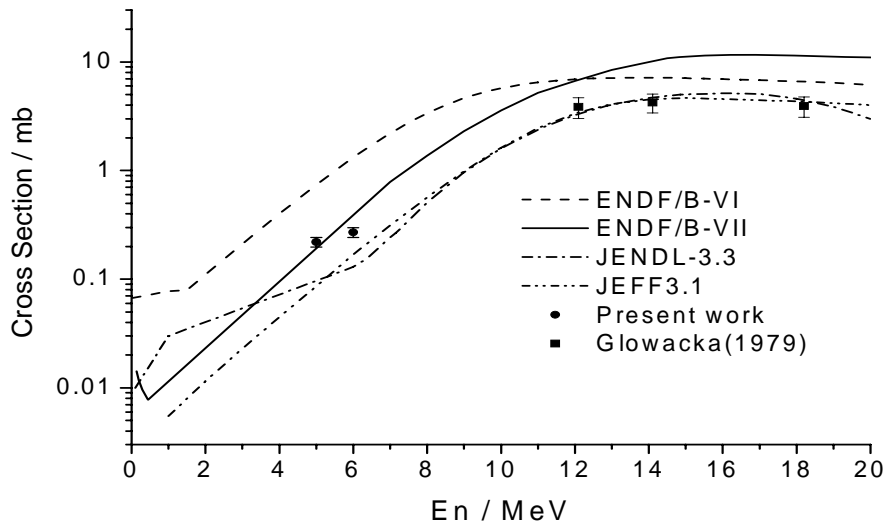


Fig. 10 Present cross sections of  $^{147}\text{Sm}(n, \alpha)^{144}\text{Nd}$  reaction

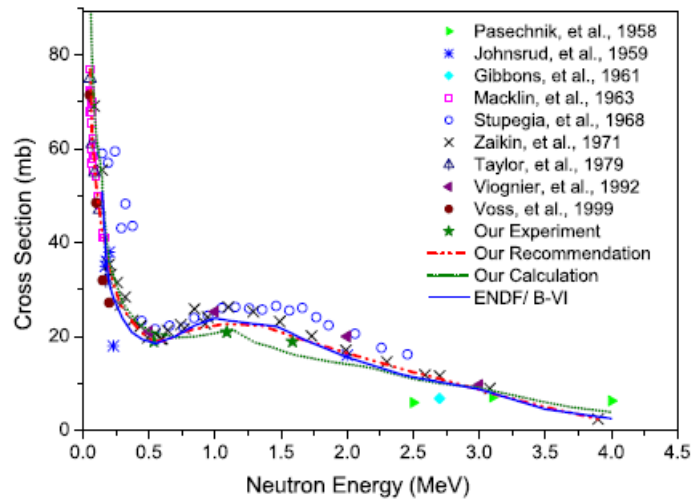


Fig. 11 Present cross sections of the  $^{141}\text{Pr}(n, \gamma)^{142}\text{Pr}$  reaction compared with existing data.

### 3. Lanzhou University:

The following cross sections was measured at neutron energy from 13.5 to 14.6 MeV at Lanzhou University by using the activation method :

$^{115}\text{In}(n, p)^{115}\text{gCd}$ ,  $^{115}\text{In}(n, \alpha)^{112}\text{Ag}$ ,  $^{115}\text{In}(n, 2n)^{114\text{m}}\text{In}$ ,  $^{113}\text{In}(n, 2n)^{112\text{m}}\text{In}$ ,  $^{115}\text{In}(n, n')^{115\text{m}}\text{In}$ ,  $^{113}\text{In}(n, n')^{113\text{m}}\text{In}$ ,  $^{128}\text{Te}(n, 2n)^{127\text{m}}\text{Te}$ ,  $^{89}\text{Y}(n, 2n)^{88}\text{Y}$ ,  $^{84}\text{Sr}(n, 2n)^{83}\text{Sr}$ ,  $^{86}\text{Sr}(n, 2n)^{85\text{m}}\text{Sr}$ ,  $^{86}\text{Sr}(n, 2n)^{85}\text{Sr}$ ,  $^{88}\text{Sr}(n, 2n)^{87\text{m}}\text{Sr}$ ,  $^{84}\text{Sr}(n, p)^{84}\text{Rb}$ ,  $^{86}\text{Sr}(n, p)^{86}\text{Rb}$ ,  $^{88}\text{Sr}(n, p)^{88}\text{Rb}$ ,  $^{82}\text{Se}(n, 2n)^{81\text{m.g}}\text{Se}$ ,  $^{76}\text{Se}(n, 2n)^{75}\text{Se}$ ,  $^{172}\text{Yb}(n, p)^{172}\text{Tm}$ ,  $^{76}\text{Se}(n, p)^{76}\text{As}$ ,  $^{74}\text{Se}(n, p)^{74}\text{As}$ ,  $^{80}\text{Se}(n, \alpha)^{77}\text{Ge}$ ,  $^{173}\text{Yb}(n, p)^{173}\text{Tm}$ ,  $^{170}\text{Yb}(n, 2n)^{169}\text{Yb}$ ,  $^{176}\text{Yb}(n, 2n)^{175}\text{Yb}$  and  $^{88}\text{Sr}(n, \alpha)^{85\text{m}}\text{Kr}$ .

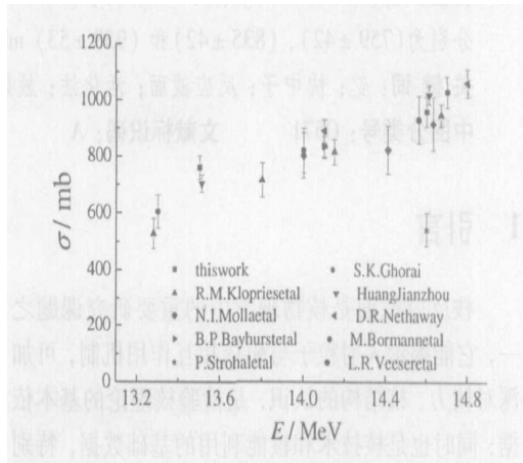


Fig.12 cross sections of  $^{89}\text{Y}(n, 2n)^{89}\text{Y}$  reaction

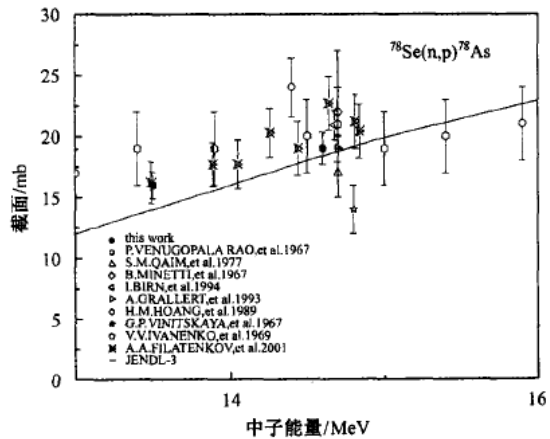


Fig.13 Data for  $^{78}\text{Se}(n, 2n)^{78}\text{As}$  reaction

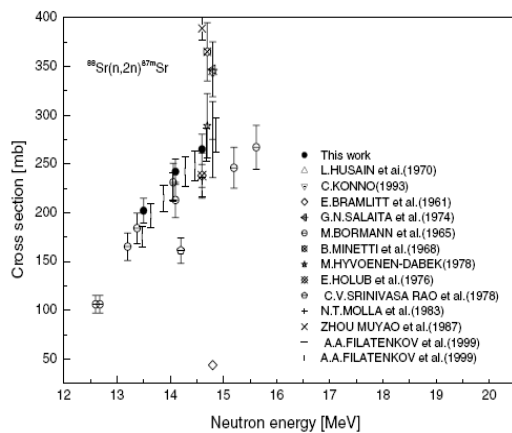


Fig.14 Data for  $^{88}\text{Sr}(n, 2n)^{87m}\text{Sr}$  reaction

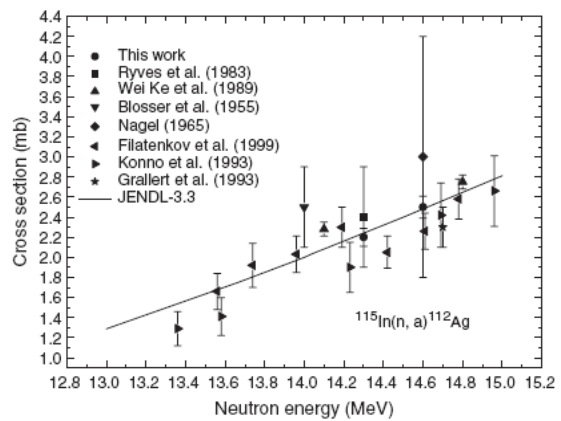


Fig.15 cross sections of  $^{115}\text{In}(n, \alpha)^{112}\text{Ag}$  reaction

## 4 Sichuan University:

The cross sections for the  $^{115}\text{In}(n, \gamma)^{116}\text{In}$ ,  $^{116m}\text{In}(n, \gamma)^{117}\text{In}$ ,  $^{71}\text{Ga}(n, \gamma)^{72}\text{Ga}$  and  $^{174}\text{Hf}(n, \gamma)^{175}\text{Hf}$  reaction were measured in neutron energy range from 30 to 1500 keV in the past years.